

Absence of a classical long-range order in $S = 1/2$ Heisenberg antiferromagnet on triangular lattice

Nobuo Suzuki,^{1,*} Fumitaka Matsubara,² Sumiyoshi Fujiki,¹ and Takayuki Shirakura³

¹*Faculty of Science and Technology, Tohoku Bunka Gakuen University, Sendai 980-8551, Japan*

²*Department of Applied Physics, Tohoku University, Sendai 980-8579, Japan*

³*Faculty of Humanities and Social Sciences, Iwate University, Morioka 020-8550, Japan*

(Dated: April 1, 2021)

We study the quantum phase transition of an $S = 1/2$ anisotropic α ($\equiv J_z/J_{xy}$) Heisenberg antiferromagnet on a triangular lattice. We calculate the sublattice magnetization and the long-range helical order-parameter and their Binder ratios on finite systems with $N \leq 36$ sites. The N dependence of the Binder ratios reveals that the classical 120° Néel state occurs for $\alpha \lesssim 0.55$, whereas a critical collinear state occurs for $1/\alpha \lesssim 0.6$. This result is at odds with a widely-held belief that the ground state of a Heisenberg antiferromagnet is the 120° Néel state, but it also provides a possible mechanism explaining experimentally observed spin liquids.

PACS numbers: 75.10.Jm, 75.40.Mg

Because an exotic spin state may occur as a result of low-dimensional quantum fluctuations and geometric frustration, the $S = \frac{1}{2}$ quantum antiferromagnetic Heisenberg (QAFH) model on the triangular lattice is one of the central issues in solid-state physics. Anderson proposed a resonating-valence-bond (RVB) state or a spin-liquid (SL) state as the ground state (GS).¹ Since then, many theoretical studies have focused on identifying the GS by using different methods such as spin-wave (SW) theory,² variational Monte Carlo techniques,^{3,4} series expansions,^{5,6} exact diagonalizations (ED) of finite systems,^{7–11} quantum Monte Carlo techniques,¹² density matrix renormalization group theory,¹³ and diagrammatic Monte Carlo techniques.¹⁴ The GS is now widely believed to be a long-range-order (LRO) state with the 120° sublattice structure (the 120° Néel state) because the results of most numerical studies can be analyzed by using this image.^{6,9,11,12} However, experimental developments have enabled us to synthesize model compounds such as κ -(ET)₂Cu₂(CN)₃,¹⁵ EtMe₃Sb[Pd(dmit)₂]₂,¹⁶ and Ba₃IrTi₂O₉.¹⁷ In these compounds, no spin ordering has been observed down at very low temperatures; several mechanisms have been proposed to resolve this discrepancy, such as spatial anisotropy,^{18,19} ring exchange,²⁰ and spinon interaction.²¹

Before examining these mechanisms, we must first carefully re-examine the GS properties of the QAFH model because the base of the 120° Néel GS is not yet solidly established. In particular, even in the most widely accepted studies, the magnitude of the sublattice magnetization (SMAG) m^\dagger is not compatible. SW theory in finite systems⁹ and the quantum Monte Carlo technique¹² suggest $m^\dagger = 0.4 \sim 0.5$ in the classical case units of $m^\dagger = 1$, whereas numerical series expansions suggest either $m^\dagger \sim 0^5$ or some small value.⁶ In the ED technique up to $N = 36$ spins, results depend on the scaling functions, which gives either $m^\dagger \sim 0.5^{9,11}$ or $m^\dagger \sim 0.10$.¹⁰ The quantum Monte Carlo technique¹² does not satisfactorily reproduce ED results for $N = 12$ and 36 .

In the present paper, we report that the GS of the

QAFH model differs from the 120° Néel state. We consider finite systems with N (≤ 36) sites in the usual way, but take a different approach. To investigate the quantum phase transition, we consider with an anisotropic model. We calculate the SMAG and the long-range helical order (LRHO) parameter and examine the Binder ratios of these quantities. We find that, in concurrence with recent results, the GS is a critical state with collinear structure in the Ising-like range and a 120° Néel state in the XY-like range. In contrast, the GS is a SL state in the Heisenberg-like range. We estimate an anisotropy threshold for the occurrence of the critical state and for the 120° Néel state.

We start with an anisotropic model on periodic finite lattices described by the Hamiltonian

$$\mathcal{H} = 2J \sum_{\langle i,j \rangle} [S_i^x S_j^x + S_i^y S_j^y + \alpha S_i^z S_j^z], \quad (1)$$

where $J > 0$, $\alpha \geq 0$, and the sum runs over all the nearest-neighbor pairs of sites. Note that the model with $\alpha = \infty$ is an Ising model for which the GS is a critical state characterized by a power law decay of the spin correlation function.²² At the other limit, the model with $\alpha \sim 0$ is an XY-like model for which the 120° Néel state is suggested to occur.^{10,23} We discuss the spin structure of the Heisenberg-like model with $\alpha \sim 1$ by comparing the properties of this model with those of the Ising- and XY-like models. The main issue is whether $m^\dagger \neq 0$ or not.

By using a power method, we calculate the GS eigenfunction $|\psi_G\rangle$ for two types of lattices, A and B, with $N \leq 36$ sites. Type-A lattices have $N = 9, 12, 21, 27, 36$, and type-B lattices have $N = 15, 18, 24, 30, 33$. The shapes of the type-A lattices were presented in Ref. 10; for this lattice type, the sublattices Ω_1, Ω_2 , and Ω_3 are equivalent. The type-B lattices are constructed so that the 120° Néel structure is possible in the classical case. The SMAG of the type-A lattices, and in particular their N dependence, have already been studied by

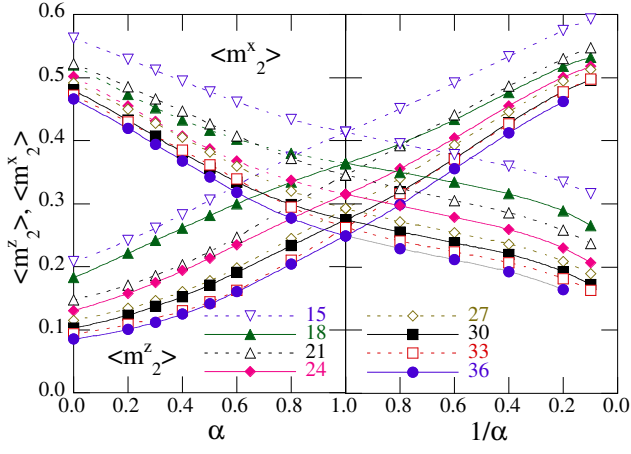


FIG. 1. (Color online) z and xy components of the SMAG ($\langle m_2^z \rangle_N$ and $\langle m_2^{xy} \rangle_N \equiv \langle m_2^{xy} \rangle_N/2$, respectively) in the GS as functions of α .

several groups.^{9–11} However, for these small systems, the data strongly depend on the parity and magnitude of N . In the present work, we add to these the data for type-B lattices.

First, we consider the SMAG. The ν component ($\nu = x, y, z$) of the square of the magnetization of the Ω_l sublattice is defined as

$$m_l^\nu = \frac{1}{(N/6)^2} \left(\sum_{i \in \Omega_l} S_i^\nu \right)^2, \quad (2)$$

and the xy component is defined as $m_l^{xy} = m_l^x + m_l^y$.

Figure 1 shows the xy and z components of the SMAGs $\langle m_2^\mu \rangle_N \equiv \frac{1}{3} \sum_i \langle m_l^\mu \rangle_N$ ($\mu = z, xy$) as functions of α , where $\langle A \rangle_N = \langle \psi_G | A(N) | \psi_G \rangle$. For $\alpha \sim 0$, $\langle m_2^{xy} \rangle_N$ has a large value and is only weakly dependent on size, whereas $\langle m_2^z \rangle_N$ is small and depends strongly on size. As α increases, $\langle m_2^{xy} \rangle_N$ gradually decreases and $\langle m_2^z \rangle_N$ increases, and $\langle m_2^z \rangle_N = \langle m_2^{xy} \rangle_N/2$ at $\alpha = 1$. The reverse is true for $1/\alpha \sim 0$. The results at $\alpha \sim 0$ and $1/\alpha \sim 0$ seem to be compatible with the classical picture of the GS. However, in contrast with the classical case, $\langle m_2^z \rangle_N$ (or $\langle m_2^{xy} \rangle_N$) does not abruptly increase (or decrease) as α is increased across the Heisenberg point $\alpha = 1$.

We now examine the quantum phase transition of the model by considering the dependence of α on $\langle m_2^z \rangle_N$ and $\langle m_2^{xy} \rangle_N$. The SMAG at $\alpha = 1$ for $N \rightarrow \infty$ has been estimated by several groups^{9–11} who used different scaling relations. However, the result depends on both the units of the sublattice magnetization and the scaling functions. Here we consider the Binder ratios²⁴ of $\langle m_2^z \rangle_N$ and $\langle m_2^{xy} \rangle_N$ which are free from the scaling function and their units. The Binder ratios of $\langle m_2^z \rangle_N$ and $\langle m_2^{xy} \rangle_N$, $B_m^z(N)$ and $B_m^{xy}(N)$, respectively, are defined as

$$B_m^z(N) = (3 - \langle m_4^z \rangle_N / \langle m_2^z \rangle_N^2) / 2, \quad (3)$$

$$B_m^{xy}(N) = (5 - 3 \langle m_4^{xy} \rangle_N / \langle m_2^{xy} \rangle_N^2) / 2, \quad (4)$$

where $\langle m_4^\mu \rangle_N \equiv \frac{1}{3} \sum_l \langle \psi_G | (m_l^\mu)^2 | \psi_G \rangle$.

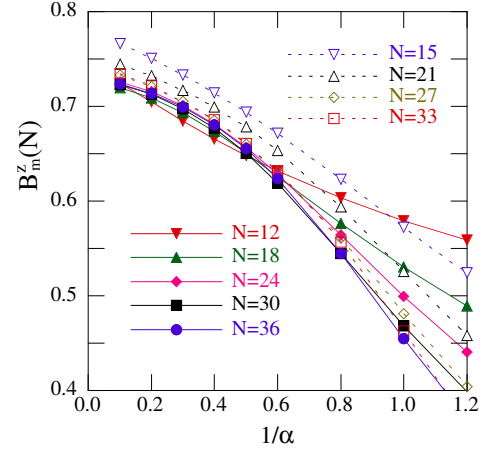


FIG. 2. (Color online) Binder ratios $B_m^z(N)$ as functions of $1/\alpha$. The ratios for N even and odd are shown by solid and open symbols, respectively.

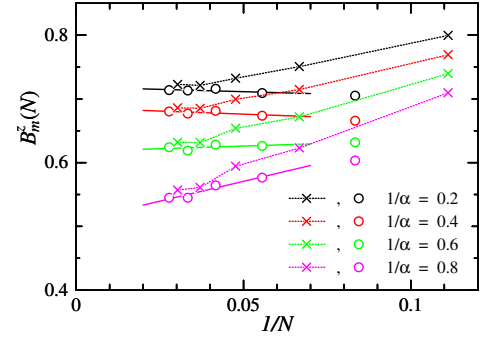


FIG. 3. (Color online) Binder ratios $B_m^z(N)$ for different $1/\alpha$ as functions of $1/N$. Ratios for N even and odd are shown by circles and crosses, respectively. The straight lines for N even are the least square fits for $N \ge 18$.

We first examine the GS of the Ising-like model for $1/\alpha < 1$. In Fig. 2, we plot $B_m^z(N)$ as functions of $1/\alpha$. The dependence of $B_m^z(N)$ on N differs somewhat for N odd or even. For N even, $B_m^z(N)$ at $1/\alpha \sim 1$ decreases with increasing N , revealing that $\langle m_2^z \rangle_N$ vanishes as $N \rightarrow \infty$. As $1/\alpha$ decreases, $B_m^z(N)$ for different N increase, come together at $1/\alpha \sim 0.6$, and then gradually increase thereafter. This result is consistent with the fact that the GS is critical at $1/\alpha = 0$.²² For N odd, although $B_m^z(N)$ are larger than for N even, even at $1/\alpha \sim 0$ they decrease with increasing N . To resolve this discrepancy, we show in Fig. 3 a plot of $B_m^z(N)$ as functions of $1/N$. We see that, as N increases, $B_m^z(N)$ for odd N approaches to those for even N . Thus, we conclude that the decrease of $B_m^z(N)$ for small N is an abnormal finite-size effect that comes from the difference in the ratio $r_z = M_z/N$, with M_z being the z component of the total-spin number.²⁵ The slopes of the fitting lines of $B_m^z(N)$ vs. $1/N$ shown in Fig. 3 are almost zero for $1/\alpha \lesssim 0.6$. We suggest that the GS is the critical state for $\alpha > \alpha_c^z$ with $1/\alpha_c^z \sim 0.6$.

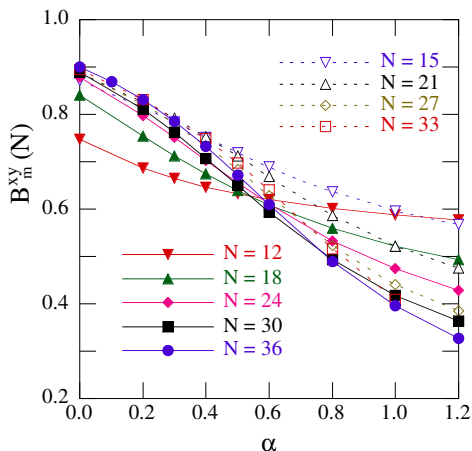


FIG. 4. (Color online) Binder ratios $B_m^{xy}(N)$ as functions of α . Ratios for N even and odd are shown by solid and open symbols, respectively.

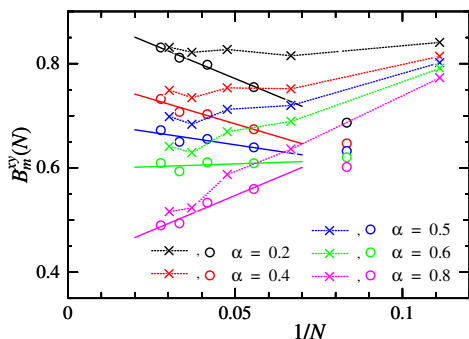


FIG. 5. (Color online) Binder ratios $B_m^{xy}(N)$ for different α as functions of $1/N$. Ratios for N even and odd are shown by circles and crosses, respectively. The straight lines for N even are the least square fits for $N \geq 18$.

Next we examine the GS of the XY-like model for $\alpha < 1$. Figures 4 and 5 show plots of $B_m^{xy}(N)$ as functions of α and of $1/N$, respectively. We see in Fig. 5 that $B_m^{xy}(N)$ for N odd also exhibit the abnormal finite-size effect; they take on values larger than those for N even, and approach the N -even values as N increases. We thus consider the dependence of $B_m^{xy}(N)$ on N for N even. At $\alpha \sim 0$, $B_m^{xy}(N)$ increases with N . This result is consistent with the recently reported presence of the LRO in the XY model.¹⁰ However, at $\alpha \sim 1$, $B_m^{xy}(N)$ decreases with increasing N , which reveals that $\langle m_2^{xy} \rangle_N$ vanishes as $N \rightarrow \infty$. The most remarkable point is that $B_m^{xy}(N)$ for different N cross at $\alpha \sim 0.55$ (see also Fig. 5). Thus, we suggest that a quantum phase transition between the SL state and the LRO state occurs at $\alpha = \alpha_c^{xy} (\sim 0.55)$.

We now consider the helicity, which gives a complementary view of the spin ordering (i.e., it is sensitive to the 120° structure). The local helicity⁷ for each upright triangle at \vec{R} is defined by

$$\vec{\chi}(\vec{R}) = \frac{2}{\sqrt{3}}(\vec{S}_i \times \vec{S}_j + \vec{S}_j \times \vec{S}_k + \vec{S}_k \times \vec{S}_i). \quad (5)$$

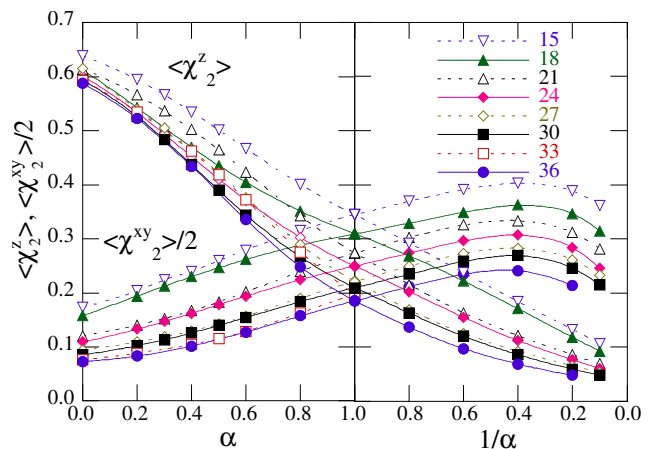


FIG. 6. (Color online) z and xy components of LRHO parameter ($\langle \chi_2^z \rangle_N$ and $\langle \chi_2^{xy} \rangle_N$, respectively) in the GS as functions of α .

The order of $i \rightarrow j \rightarrow k$ is counterclockwise. The LRHO parameter in the ν component is defined as

$$\chi_2^\nu = \frac{1}{N^2} \left(\sum_{\vec{R} \in \Delta} \chi^\nu(\vec{R}) \right)^2, \quad (6)$$

where the sum is over all upright triangles. We consider the LRHO parameter in the xy plane, χ_2^z , and in a plane orthogonal to the xy plane (hereinafter called the yz plane), $\chi_2^{xy} (= \chi_2^x + \chi_2^y)$. Note that χ_2^z was already calculated by several authors.^{7,10,23} Here we add χ_2^{xy} to examine the occurrence of a distorted 120° structure in the yz plane. In the classical case, $\chi_2^z = 1$ and $\chi_2^{xy} = 0$ for $0 \leq \alpha < 1$, whereas $\chi_2^z = 0$ and $\chi_2^{xy} \lesssim 1$ for $1/\alpha \lesssim 1$ (i.e., χ_2^z and χ_2^{xy} suddenly exchange their role at $\alpha = 1$).

Figure 6 shows $\langle \chi_2^z \rangle_N$ and $\langle \chi_2^{xy} \rangle_N$ as functions of α . We see that $\langle \chi_2^z \rangle_N$ has properties similar to those of $\langle m_2^{xy} \rangle_N$: it takes on a large value at $\alpha \sim 0$ and decreases with increasing α . However, the dependence of $\langle \chi_2^{xy} \rangle_N$ on α differs somewhat from that of $\langle m_2^z \rangle_N$; although it increases with α , its increment is suppressed for $\alpha > 1$ ($1/\alpha < 1$). In particular, it reaches a maximum at $1/\alpha \sim 0.4$ and then decreases. This is a consequence of the spin state becoming collinear at the Ising limit $1/\alpha \rightarrow 0$. Note that, even for $1/\alpha \sim 0.4$, $\langle \chi_2^{xy} \rangle_N$ depends strongly on N , which reveals the absence of the xy -component LRHO in this model. That is, the critical state for $\alpha > \alpha_c^z$ has a collinear spin structure along the z -axis. A remarkable point is that, like $\langle m_2^z \rangle_N$ and $\langle m_2^{xy} \rangle_N$, $\langle \chi_2^z \rangle_N$ and $\langle \chi_2^{xy} \rangle_N$ for $\alpha < 1$ are smoothly connected with those for $\alpha > 1$. This result supports the finding above that the spin structure does not change abruptly at the Heisenberg point $\alpha = 1$.

To examine the presence of the 120° structure in the xy plane, we consider the Binder ratio $B_\chi^z(N)$ of $\langle \chi_2^z \rangle_N$, which is defined as

$$B_\chi^z(N) = (3 - \langle \chi_4^z \rangle_N / \langle \chi_2^z \rangle_N^2) / 2. \quad (7)$$

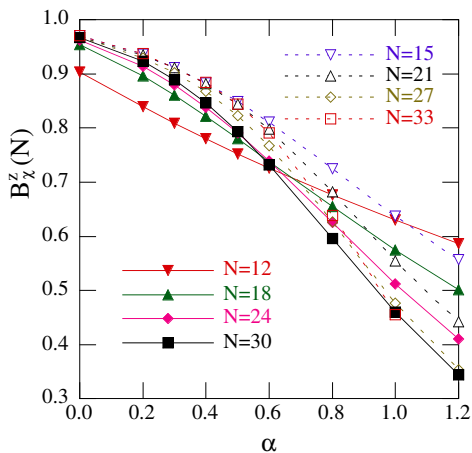


FIG. 7. (Color online) Binder ratios B_χ^z as functions of α . Ratios for N even and odd are shown by solid and open symbols, respectively.

Figure 7 shows plots of $B_\chi^z(N)$ as functions of α . We see that $B_\chi^z(N)$ exhibit properties quite similar to $B_m^{xy}(N)$; the abnormal finite-size effect of $B_\chi^z(N)$ for N odd, at $\alpha \sim 1$ $B_\chi^z(N)$ is smaller as N increases, and at $\alpha \sim 0$ the reverse is true. The most interesting point is that $B_\chi^z(N)$ for different N even intersect at $\alpha \sim 0.6$. This value of

$\alpha \sim 0.6$ is consistent with the critical value $\alpha_c^{xy} \sim 0.55$ that is estimated from $B_m^{xy}(N)$. That is, the LRHO accompanies the LRO of the SMAG. Thus, we conclude that a quantum phase transition from the SL state to the 120° Néel state occurs at $\alpha = \alpha_c^{xy} \sim 0.55$. We should note, however, that further studies are necessary to establish the critical value of α_c^{xy} as well as that of α_c^z .

We thus studied the GS property of the anisotropic quantum antiferromagnetic Heisenberg (QAFH) model on a finite triangular lattice with $N \leq 36$ sites. We find that the GS of the model is the 120° Néel state for $\alpha < \alpha_c^{xy} (\sim 0.55)$ and is the critical collinear state for $1/\alpha < 1/\alpha_c^z (\sim 0.6)$. That is, classical LRO is absent at $\alpha \sim 1$. Although this result contrasts strongly with recent theoretical ideas, it is consistent with recent experiments. We hope that our results will stimulate both theoretical and experimental works in low-dimensional frustrated quantum systems.

ACKNOWLEDGMENTS

Part of the results in this research was obtained using the supercomputing resources at Cyberscience Center, Tohoku University.

* nobu@ait.tbgu.ac.jp

¹ P. W. Anderson, Mat. Res. Bull. **8**, 153 (1973).

² S. J. Miyake, J. Phys. Soc. Jpn. **61**, 983 (1992), and references there in.

³ D. A. Huse and V. Elser, Phys. Rev. Lett. **60**, 2531 (1988).

⁴ P. Sindzingre, P. Lecheminant, and C. Lhuillier, Phys. Rev. B **50**, 3108 (1994).

⁵ R. R. P. Singh and D. A. Huse, Phys. Rev. Lett. **68**, 1766 (1992).

⁶ N. Elstner, R. R. P. Singh, and A. P. Young, Phys. Rev. Lett. **71**, 1629 (1993).

⁷ S. Fujiki and D. D. Betts, Can. J. Phys. **65**, 76 (1987); **65**, 489 (1987); Suppl. Prog. Theor. Phys. **87**, 268 (1986).

⁸ H. Nishimori and H. Nakanishi, J. Phys. Soc. Jpn. **57**, 262 (1988); **58**, 2607 (1989); **58**, 3433 (1989).

⁹ B. Bernu, C. Lhuillier, and L. Pierre, Phys. Rev. Lett. **69**, 2590 (1992); B. Bernu, P. Lecheminant, C. Lhuillier, and L. Pierre, Phys. Rev. B **50**, 10048 (1994).

¹⁰ P. W. Leung and K. J. Runge, Phys. Rev. B **47**, 5861 (1993).

¹¹ J. Richter, J. Schulenburg, A. Honecker, and D. Schmal-fuss, Phys. Rev. B **70**, 174454 (2004).

¹² L. Capriotti, A. E. Trumper, and S. Sorella, Phys. Rev. Lett. **82**, 3899 (1999).

¹³ S. R. White and A. L. Chernyshev, Phys. Rev. Lett. **99**, 127004 (2007).

¹⁴ S. A. Kulagin, N. Prokof'ev, O. A. Starykh, B. Svistunov, and C. N. Varney, Phys. Rev. Lett. **110**, 070601 (2013).

¹⁵ Y. Shimizu, K. Miyagawa, K. Kanoda, M. Maesato, and G. Saito, Phys. Rev. Lett. **91**, 107001 (2003).

¹⁶ T. Itou, A. Oyamada, S. Maegawa, M. Tamura, and R. Kato, Phys. Rev. B **77**, 104413 (2008).

¹⁷ T. Dey, A. V. Mahajan, P. Khuntia, M. Baenitz, B. Koteswararao, and F. C. Chou, Phys. Rev. B **86**, 140405(R) (2012).

¹⁸ H. Morita, S. Watanabe, and M. Imada, J. Phys. Soc. Jpn. **71**, 2109 (2002).

¹⁹ S. Yunoki and S. Sorella, Phys. Rev. B **74**, 014408 (2006).

²⁰ O. I. Motrunich, Phys. Rev. B **72**, 045105 (2005).

²¹ S.-S. Lee, P. A. Lee, and T. Senthil, Phys. Rev. Lett. **98**, 067006 (2007).

²² J. Stephenson, J. Math. Phys. **5**, 1009 (1964).

²³ N. Suzuki and F. Matsubara, Phys. Rev. B **51**, 6402 (1995).

²⁴ K. Binder, Z. Phys. B **48**, 319 (1982).

²⁵ As r_z increases, B_m^z increases because the number of basis states decreases. For N odd, $r_z (= 1/2N)$ decreases with increasing N , which weakens the effect, and it is absent for N even.